Exploring the binding pocket of quinone/inhibitors in mitochondrial respiratory complex I by chemical biology approaches

Running title: Chemical biology of respiratory complex I

Masatoshi Murai *

Division of Applied Life Sciences, Graduate School of Agriculture, Kyoto University, Sakyo-ku, Kyoto 606-8502, Japan

*To whom correspondence should be addressed: m_murai@kais.kyoto-u.ac.jp

ABSTRACT

NADH-quinone oxidoreductase (respiratory complex I) is a key player in mitochondrial energy metabolism. The enzyme couples electron transfer from NADH to quinone with the translocation of protons across the membrane, providing a major proton-motive force that drives ATP synthesis. Recently, X-ray crystallography and cryo-electron microscopy provided further insights into the structure and functions of the enzyme. However, little is known about the mechanism of quinone reduction, which is a crucial step in the energy coupling process. A variety of complex I inhibitors targeting the quinone-binding site have been indispensable tools for mechanistic studies on the enzyme. Using biorationally designed inhibitor probes, the author has accumulated a large amount of experimental data characterizing the actions of complex I inhibitors. On the basis of comprehensive interpretations of the data, the author reviews the structural features of the binding pocket of quinone/inhibitors in bovine mitochondrial complex I.

Key words: *Respiratory complex I, mitochondria, inhibitor, ubiquinone, chemical biology.*

Abbreviations **:** ATP; adenosine triphosphate, BODIPY; boron dipyrromethene, complex I; proton-translocating NADH-quinone oxidoreductase, EM; electron microscopy, FeS; iron-sulfur, FMN; flavin adenine mononucleotide, LDT; ligand-directed tosylate, NADH; nicotinamide adenine dinucleotide, ROS; reactive oxygen species, SMP; submitochondrial particle, TAMRA; 6-carboxy-*N,N,N',N'*-tetramethylrhodamine, THF; tetrahydrofuran, TMH; transmembrane helix.

Introduction

The mitochondrion is an organelle that plays a crucial role in oxidative phosphorylation, a process whereby ATP is generated as a result of electron transfer from NADH to oxygen through a series of respiratory enzymes (*1*). In most eukaryotic cells, proton-translocating NADH-quinone oxidoreductase (respiratory complex I) catalyzes an initial step in the mitochondrial respiratory chain. Complex I couples electron transfer from NADH to quinone with the translocation of protons across the biological membrane, contributing to the proton motive force for ATP synthesis (*2-5*).

Complex I is the largest, most complicated, and least understand enzyme of the respiratory chain. The enzyme from bovine heart mitochondria comprises 45 different subunits with a molecular mass of ~1 MDa (*6*); the highly conserved 14 "core" subunits are crucial for the enzyme catalysis (see also Table S1), whereas the 31 mammalian-specific "supernumerary" subunits are thought to be involved in assembly of the protein complex and/or regulation of the catalytic cycle (*7, 8*). Complex I has a unique L-shaped structure, which is composed of two major domains called "hydrophilic" and "membrane" domains (Figure 1). The hydrophilic domain, where electron transfer takes place, protrudes into the mitochondrial matrix side, while the membrane domain, where proton-translocation takes place, is embedded in the plane of the inner membrane (*2-5*).

Complex I is known to be a major source of cellular reactive oxygen species (ROS, *9-11*), which are associated with various pathologies such as diabetes, cardiovascular disease, neurodegeneration, and cancer (*12, 13*). ROS are produced when the catalytic functions of complex I are disrupted by point mutations or inhibitors like a neurotoxin *N*-methyl-4-phenylpyridinium (MPP^+, *14, 15*). More recently, *in vivo* and *ex vivo* studies demonstrated that the accumulation of succinate in the mitochondrial matrix under hypoxic conditions accelerates ROS production from complex I, which leads to the severe oxidative damage called ischemia-reperfusion injury (*16, 17*). However, the site and mechanism of ROS production in complex I remain largely debatable because fundamental knowledge of the structure and function of complex I is still limited.

From a historical point of view, mode of action studies of specific inhibitors targeting respiratory enzymes have provided valuable insights into the structure and function (*18, 19*). A variety of naturally occurring or synthetic chemicals are known to inhibit the catalytic activity of complex I at the nM level. Some of them, such as rotenone and piericidin families, have been indispensable tools for mechanistic studies of the enzyme because they are believed to act at the quinone-binding site, where the quinone reduction is coupled to proton translocation (*3-5*).

Complex I has also been successfully exploited as a promising druggable target. Synthetic chemicals such as fenpyroximate and pyridaben have been developed as excellent insecticides targeting complex I in agricultural pests (*20*). The anthelmintic compound nafuredin, which was isolated from the fermentation broth of *Aspergillus niger* FT-0554, has been reported as a selective inhibitor of complex I from the parasitic helminth *Ascaris suum (21)*. Moreover, there have been interesting reports that anti-diabetic, anti-inflammatory, and anti-tumor effects of some therapeutic reagents are attributable to complex I inhibition, which alters the cellular energy states or metabolic profiles (*22-25*). Therefore, detailed characterization of the actions of inhibitors targeting complex I will provide valuable information not only on the structure and functions of complex I, but also on drug design strategies.

Herein, the author focuses on the following three topics including findings obtained by chemical biology approaches using biorationally designed inhibitors as molecular probes: (i) identification of the inhibitor-binding sites in complex I by photoaffinity labeling, (ii) an overview of the binding pocket of quinone/inhibitor in complex I, and (iii) probing the binding pocket of quinone/inhibitor through specific chemical modifications.

Identification of the inhibitor-binding site(s) by photoaffinity labeling

Background

There is a general consensus that quinone reduction is a crucial step in the reaction of complex I because it couples to triggering proton translocation across the membrane (*2-5*). A wide variety of complex I inhibitors, with a few exceptions of flavin-site inhibitors such as Rhein (an anthraquinone derivative) and DPI (diphenyleneiodonium), are generally called "quinone-site inhibitors" because they inhibit enzyme activity by occupying the quinone-binding site (*18, 19*). However, at the time the author started the research, there was no consensus on the position or number of binding sites for quinone/inhibitor since structural information on complex I was limited.

A photoaffinity labeling technique, which employs a synthetic ligand possessing a photolabile group such as diazirine and phenyl azido, is the most commonly used methodology for specific chemical modifications of proteins (*26, 27*). It provides a powerful means of investigating interactions between biologically active compounds and proteins of interest. To identify the quinone/inhibitor-binding site(s) in complex I, photoaffinity labeling with bovine heart submitochondrial particles (SMPs) was carried out using various inhibitors such as acetogenin, quinazoline, fenpyroximate, and amilorides as templates (Figure 2) (*28-34*). These labeling studies, for the first time, provided an overview of the quinone/inhibitor-binding site in mitochondrial complex I as follows.

The binding site of acetogenins

Acetogenins isolated from the plant species Annonaceae, such as bullatacin and rollininstatin-1, are among the most potent inhibitors of bovine complex I (*18*). We designed and synthesized two photoreactive acetogenins ([^{125}I]TDA and [^{125}I]DANA, Figure 2a), which possess a photolabile phenyl diazirine in place of the toxophoric γ-lactone ring and a small diazirine in the vicinity of the toxopholic bis-THF ring moiety, respectively. The two photoreactive acetogenins specifically labeled the hydrophobic

ND1 subunit, which is located at the junction of the hydrophilic and membrane domains (Figure 1) (*28, 31*). The proteolytic analysis of the ND1 subunit labeled by [^{125}I]TDA and [^{125}I]DANA revealed that the γ-lactone ring and bis-THF moiety of acetogenin bind the region covering TMH4−5 and the matrix side third loop connecting TMH5−6, respectively (Figures 3a and S1a, *30, 32*). These results are the first direct evidence that the ND1 subunit constructs the inhibitor binding site in complex I.

The binding site of quinazoline-type inhibitors

Quinazoline-type chemicals including 6-amino-4-(4-*tert*-butylpheneythylamino)quinazoline (AQ) are other potent inhibitors of complex I. They have been recognized as important chemical tools for complex I research because they inhibit not only mammalian complex I but also enzymes from the aerobic yeast *Yarrowia lipolitica* and parasitic helminth *A. suum* (*35-37*). We synthesized a photoreactive quinazoline ([^{125}I]AzQ, Figure 2b), which possesses a photolabile azido group on the toxophoric quinazoline ring. [^{125}I]AzQ labeled both the hydrophilic 49-kDa and hydrophobic ND1 subunits at a ratio of ~4:1 (*29*). The regions labeled by [^{125}I]AzQ in the 49-kDa and ND1 subunits were determined to be the N-terminal region (Asp41-Arg63) and the matrix-side third loop connecting TMH5−6, respectively, suggesting that the two regions are close to each other (Figures 3a and S1b, *33*). Our observations underline the functional significance of the interfacial region between the hydrophilic and hydrophobic domains, which is considered to be a key player in quinone reduction and energy transduction.

The binding site of fenpyroximate

Fenpyroximate has been used as an acaricide targeting complex I of mites (*19*). We carried out photoaffinity labeling studies using two photoreactive fenpyroximates ([^{125}I]APF and [^{125}I]AIF, Figure 2c) possessing a photoreactive azido group at and far from the toxophoric pyrazole ring moiety, respectively (*34*). [^{125}I]APF and [^{125}I]AIF

specifically labeled the hydrophilic PSST and 49-kDa subunits, respectively, suggesting that fenpyroximate binds to the interface between the two. Careful proteomic analyses of the labeled subunits revealed that the regions labeled by [^{125}I]APF and [^{125}I]AIF are located in the peptide Ser63-Arg66 in the PSST subunit and Asp160-Arg174 in the 49-kDa subunit, respectively, which construct the putative quinone/inhibitor-binding pocket (Figures 3a and S1c, *34*). These results demonstrate that fenpyroximate binds to the interface of the two regions in a manner such that the toxophoric pyrazole ring and side chain orient toward the PSST and 49-kDa subunits, respectively.

Together with the results on the photoreactive acetogenins and quinazoline, it is clear that chemically diverse inhibitors commonly bind to the interfacial region between hydrophilic and hydrophobic domains, which comprises the 49-kDa, PSST, and ND1 subunits, but in markedly different manners reflecting their chemical structures (Figure 3a). This view about the binding pocket of quinone/inhibitor in complex I was later supported by the structural work on *Thermus thermophilus* complex I (*38*).

The binding site of amilorides

The diuretic drug amiloride and its analogues, such as commercially available EIPA, MIA, and benzamil (Figure 2d), are well-known inhibitors of Na^+/H^+ and Na^+/Ca^+ antiporters and Na^+ channels (*39, 40*). They have also been shown to inhibit bacterial and mitochondrial complex I, but their inhibitory potencies, in terms of IC_{50} values, are much weaker than those of conventional quinone-site inhibitors such as acetogenin and quinazoline (*41, 42*). As the membrane subunits ND2, ND4, and ND5 are homologous to the bacterial Mrp-type Na^+/H^+-antiporters (*43, 44*), amilorides have long been considered to bind to any or all of the antiporter-like subunits. However, there is no direct experimental evidence to support this.

Commercially available amilorides are not suitable for design templates for the synthesis of photoreactive amilorides due to their weak inhibition of complex I. Through comprehensive structure-activity relationship studies on amilorides as complex

I inhibitors *(45)*, we succeeded in producing four potent photoreactive amilorides, which possess a photolabile azido group in the toxophoric pyrazinoyl ring ([^{125}I]PRA4 and [^{125}I]PRA6, Figure 2d) or in the side chain moiety ([^{125}I]PRA3 and [^{125}I]PRA5, Figure 2d), respectively (*46*). [^{125}I]PRA3 and [^{125}I]PRA4 have a prototypical guanidine skeleton, which is thought to be crucial in inhibitors of various antiporters and channels (*39, 40*). [^{125}I]PRA5 and [^{125}I]PRA6 are amide-type amiloride derivatives that elicit more potent inhibitory activities than prototypical guanidine-type derivatives with bovine complex I (*47*).

Contrary to our initial expectations, the photoreactive amilorides labeled none of the antiporter-like subunits; they specifically labeled the interfacial region of bovine complex I formed by the multiple core subunits (49-kDa, PSST, and ND1) and the 39-kDa supernumerary subunit (Figure 3b) The specific binding of the four photoreactive amilorides to the target subunits was markedly suppressed in the presence of excess short-chain ubiquinones or quinone-site inhibitors such as acetogenin, quinazoline, and fenpyroximate. These results clearly demonstrate that amilorides bind to the quinone binding pocket in complex I, rather than directly blocking its activity by binding antiporter-like subunits (*46*). Furthermore, as discussed in the next section, the labeling study provided the first evidence that the supernumerary 39-kDa subunit, together with the core 49-kDa, PSST, and ND1 subunits, comprises the binding pocket of quinone/inhibitor.

An overview of the binding pocket of quinone/inhibitor in complex I

An overall structure of respiratory complex I

In 2013, the entire structure of complex I from an aerobic hyper-thermophilic bacteria *Thermus thermophilus* was determined by X-ray crystallography at a 3.3 Å resolution, revealing how the 14 conserved core subunits and cofactors are arranged (*38*). The hydrophilic domain (7 subunits: 51-kDa, 24-kDa, 75-kDa, 49-kDa, 30-kDa, PSST, and TYKY) contains one non-covalently-bound FMN and seven Fe-S clusters, which are responsible for electron transfer from NADH to quinone (Figure 1a). The membrane domain (7 subunits: ND1, ND2, ND3, ND4, ND4L, ND5, and ND6) includes the three largest antiporter-like subunits ND2, ND4, and ND5, which are arranged towards the distal end of the domain. As these three subunits show sequence similarity with MrpA (ND5 homolog) and MrpD (ND2 and ND4 homologs) subunits of bacterial Mrp-type Na^+/H^+-antiporter (MrpA to G, *43, 44*), they are likely to contribute to proton translocation. The overall architecture of complex I suggests the mechanism of redox-driven proton translocation by complex I: the quinone reduction at the interface between hydrophilic and membrane domains may induce some conformational changes in the region, which are transmitted to the antiporter-like subunits, resulting in the translocation of protons (*3-5*).

On the basis of the crystal structure of *T. thermophilus* complex I, the architectures of the 14 core subunits of mitochondrial complex I from yeast (*Y. lipolitica, 48*) and bovine heart (*49*) have been determined at moderate resolutions by X-ray crystallography and single-particle cryo-electron microscopy (cryo-EM), respectively. More recently, the entire structures of mammalian mitochondrial complexes I from bovine (*50, 51*), ovine (*Ovis aries*, *52*), porcine (*Susscrofa domesticus*, *53*), and mouse (*Mus musculus*, *54*) hearts and human (*Homo sapiens*) HEK293F cells (*55*) were modeled by cryo-EM, clarifying the locations of all 45 subunits including the assignment of 31 supernumerary subunits (Figure 1b).

Architecture of quinone-access channel

One of the notable findings obtained with *T. thermophilus* complex I (*38*) is the identification of a quinone-access channel, which extends from the membrane interior to the terminal Fe-S cluster N2 (~30 Å long, Figure 1a). The channel is a completely enclosed tunnel with a narrow entry point (3~5 Å diameter) that is framed by TMH1, TMH6, and amphipathic α-helix1 from the ND1 subunit and TMH1 from the ND3 subunit. Ubiquinones with varying isoprenyl chains (UQ_1 − UQ_{10}) are considered to enter and transit the channel to be reduced at the "top" of the channel. Since the planar quinone ring is wider (~6 Å across) than the diameter of the entry point, the channel has been considered to undergo structural rearrangement to accommodate quinones in the channel (*38, 54*). The quinone-site inhibitors such as rotenone, piericidin A, and quinazoline are considered to enter the channel and block its interior (*38, 48*). Furthermore, it was revealed that the channel is linked to the network of potentially ionized or protonated residues inside the membrane domain, which may play critical roles in the transmission of conformational changes triggered by the quinone reduction and in proton translocation across the membrane (*38*). Similar structural models were reported for mammalian complex I (Figure 1b, *50, 51, 54*).

These advances in structural studies along with computational simulations (*56-58*) have provided a common consensus on the coupling mechanism of complex I: the structural and electrostatic rearrangements induced by quinone reduction, which take place inside the proposed quinone-access channel, transmit to the membrane domain via the link continuing over the domain as the central axis of potentially ionized or protonated residues to trigger the translocation of four protons (*3-5*). Thus, quinone reduction is a key event in energy conversion by complex I; however, the mechanism responsible remains elusive because the scenarios for the binding of quinones and inhibitors to the channel have yet to be experimentally verified.

Probing the binding pocket of quinone/inhibitor through specific chemical modifications

Background

As we predicted, the binding pocket of quinone/inhibitor in complex I was identified at the interfacial region between the hydrophilic and membrane domains, which is primarily composed of the 49-kDa, PSST, and ND1 subunits (Figure 3, *38, 48, 50*). However, the sites labeled by the various inhibitor probes do not completely overlap the interior of the proposed quinone-access channel (*28-34, 46*. For example, acetogenin ([^{125}I]DANA and [^{125}I]TDA) was demonstrated to bind to the ND1 subunit in a manner such that the bis-THF ring and γ-lactone are oriented toward the loop connecting TMH5-6 and the region spanning TMH4-5, respectively (Figure 3a, *30, 32*). A part of these regions comprises an entrance of the channel, but the acetogenin molecule is positioned outside the channel (Figure 3a). Furthermore, photoaffinity labeling using photoreactive amilorides revealed that they bind to the interfacial domain of multiple core subunits (49-kDa, ND1, and PSST) and the 39-kDa supernumerary subunit (Figure 3b, *46*), although the latter does not make up the channel in the current models. The results of photoaffinity labeling studies strongly suggest that the binding pocket of the quinone/inhibitor is distributed *around* the predicted channel. Based on comprehensive interpretations of our findings, we questioned whether the current channel model fully reflects catalytically relevant states of the enzyme. Therefore, we need to explore new techniques in order to elucidate the structural features of the binding pocket of quinone/inhibitors through chemical biology approaches.

Site-specific chemical modification of complex I via LDT chemistry

In an attempt to meet this challenge, we carried out site-specific chemical modifications of intact complex I via ligand-directed tosylate (LDT) chemistry. LDT chemistry, which is based on the principle of affinity labeling, is a unique technique for chemical modifications of proteins (*59*). This technique employs a labeling reagent, in

which a high affinity ligand moiety for the target protein and a synthetic tag of choice are connected by a phenyl sulfonate (tosylate) group. The tosylate group undergoes an S_N2 reaction with nucleophilic amino acids such as Cys, His, Glu, and Asp nearby the ligand binding site. We synthesized a high affinity ligand derived from acetogenins (AL2, Figure 4b) to transfer the tag to the binding pocket of quinone/inhibitor (*60*). The terminal azido in AL2 was selected as a tag to be incorporated into the enzyme because this group can serve as a "handle" for subsequent various chemical modifications (e.g., modifications by biotin or fluorophores) via a reaction called "Cu^+-catalyzed click chemistry" (azide−alkyne [3+2] cycloaddition in water, *61*).

Bovine SMPs were incubated with AL2 to achieve the modification (azidation) of complex I through LDT chemistry. Detailed proteomic analyses by means of mass spectrometry in combination with biotinylation of the modified peptides via Cu^+-catalyzed click chemistry revealed that the modification by AL2 occurs at Asp160 in the 49-kDa subunit (49-kDa Asp160, *60*), which is located in the inner part of the proposed quinone-access channel (Figures 1a and 4a). The modification was completely suppressed in the presence of an excess amount of other quinone-site inhibitors such as bullatacin, quinazoline, and fenpyroximate. Our studies demonstrated that the quinone-access channel in intact complex I can be site-specifically modified by the LDT ligand, thereby providing a positive clue into diverse chemical modifications of the enzyme in combination with click chemistry.

Pinpoint chemical modification of 49-kDa Asp160 *located inside the quinone-access channel of complex I*

Ring-strained cycloalkynes are known to covalently attach to an azido group via a reaction called "strain-promoted click chemistry" under physiological conditions, leading to a triazole product (*62, 63*). Therefore, Asp160-N_3 may serve as a "handle" for subsequent diverse chemical modifications by externally added ring-strained cycloalkynes as a second tag, which would lead to unique biochemical and/or biophysical

studies of complex I. We used a cycloalkyne possessing a bulky rhodamine fluorophore (TAMRA-DIBO, Figure 4b, *60*) as the reaction partner of the azido group incorporated into 49-kDa Asp160 (Asp160-N_3) because it is of interest to examine whether the bulky TAMRA-DIBO can directly react with Asp160-N_3 of intact complex I in SMPs. Notably, TAMRA-DIBO directly reacted with Asp160-N_3. Short-chain ubiquinones and an excess amount of quinone-site inhibitors did not interfere with the reaction between TAMRA-DIBO and Asp160–N_3.

We also synthesized various LDT ligands using bullatacin as a template, which possess different first tags to be incorporated into 49-kDa Asp160, and examined reactivities against externally added second tags (*60*). We found that instead of strain-promoted click chemistry, reverse-electron-demand Diels-Alder cycloaddition (*64*) of a pair of cyclopropene (*65*) incorporated into 49-kDa Asp160 (via LDT chemistry using AL6, Figure 4b) and externally added BODIPY-tetrazine (Figure 4b) is more efficient for the pinpoint modification (*66*). We also noted that excess quinone-site inhibitors did not interfere with Diels-Alder cycloaddition between the cyclopropene and tetrazine.

Physiological relevance of the quinone-access channel model

The findings through the modifications of complex I are difficult to reconcile with the quinone-access channel model derived from the structural studies (*38, 48, 50, 52*); the channel (~30 Å long cavity) is completely shielded from water with only a narrow entry point (3~5 Å diameter) for quinone/inhibitors (Figure 1). If there is only one entry point for quinone/inhibitors, as modeled, bulky TAMRA-DIBO and BODIPY-tetrazine have to enter through the narrow entry point and transit the channel to react with the 49-kDa Asp160 modified by AL2 and AL6, respectively (Figure 4). However, we considered the possibility of this to be very low because these bulky second tags are much larger than the minimal diameter of the channel. Moreover, if excess quinone or quinone-site inhibitors occupy the channel, these tags may be unable to come into close proximity with 49-kDa Asp160; but this was also not the case (*60, 66*).

Thus, our observations are difficult to reconcile with the current quinone-access channel model (*38, 48, 50, 52*) unless the channel undergoes large structural rearrangement to allow bulky ligands into the proximity of 49-kDa Asp160. The channel was originally postulated to undergo slight structural rearrangement since the planar UQ ring is wider than the minimal diameter of the channel (*38, 54*). However, the structural rearrangement required for the modification by TAMRA-DIBO or BODIPY-tetrazine should be much more marked than the originally proposed one, because these ligands are much wider than the channel entrance and body.

With the results above and those obtained by photoaffinity labeling experiments, it is likely that the binding pocket of the quinone/inhibitor is considerably "open" to allow a wide range of ligands access to the deep inside. The putative open access path may be located in the area where the regions labeled by different types of photoreactive inhibitors, including acetogenin (*30, 32*), quinazoline (*29, 33*), fenpyroximate (*34*), and amilorides (*46*), are in contact or close to one other. We tentatively propose a potential common entry area of the open path, as marked by the yellow circle in Figure 3b, because all these photoreactive inhibitors examined were competitive with each other. This area is not only closer to the terminal Fe-S cluster N2 than the predicted channel entrance but also includes or is in close contact with loops connecting TMH5−6 in the ND1 and that connecting TMH1−2 in the ND3. Based on the current structural model of complex I, there is not enough space for quinones and inhibitors in this area because these loops shield the quinone-reaction site (or 49-kDa Asp160), although a part of the loops is disordered to varying degrees. These flexible loops may be dynamic "lids" that allow a variety of ligands including quinones to access the reaction site rather than rigid "walls" that enclose the site.

Conclusion

We have characterized the binding pocket of quinones/inhibitors in mitochondrial respiratory complex I through chemical biology approaches. Our photoaffinity labeling studies first revealed that chemically diverse complex I inhibitors bind to the interfacial region between hydrophilic and hydrophobic domains of the enzyme, which mainly comprises the 49-kDa, PSST, and ND1 subunits. Furthermore, we achieved the pinpoint chemical modification of the 49-kDa Asp160, which is located deep inside the quinone-access channel, via two-step conjugation reactions. Interestingly, in contrast to the channel model proposed by X-ray crystallographic and cryo-EM studies, our studies strongly suggest that the channel undergoes marked structural rearrangements to allow a variety of ligands access to the deep inside. In order to clarify whether the channel model fully reflects the physiologically relevant state of complex I, structures of the enzyme under different conditions (e.g., quinone-bound or different inhibitor-bound states) with higher resolution are needed to solve the current contradictions.

Acknowledgements

This review article is a summary of work that received the "JSBBA Award for Young Scientists". The study presented in this review was carried out at the Graduate School of Agriculture, Kyoto University. I sincerely thank Prof. Dr. Hideto Miyoshi (Kyoto University) for continuous supervision, valuable discussion, and encouragement throughout this research. I would also like to express my gratitude to all the collaborators and colleagues who have worked together for their kind support.

References

1. Rich PR, Marechal A. Electron transfer chains: structures, mechanisms and energy coupling. Comp. Biophys. 2012;8:73-93.
2. Brandt U. Energy converting NADH:quinone oxidoreductase (complex I). Annu. Rev. Biochem. 2006;75:69-92.
3. Hirst J. Mitochondrial complex I. Annu. Rev. Biochem. 2013;82:551-575.
4. Sazanov LA. A giant molecular proton pump: structure and mechanism of respiratory complex I. Nat. Mol. Cell. Biol. 2015;16:375-388.
5. Wirth C, Brandt U, Hunte C, et al. Structure and function of mitochondrial complex I. *Biochim. Biophys. Acta* 2016;1857:902-914.
6. Hirst J, Carroll J, Fearnley, IM, et al. The nuclear encoded subunits of complex I from bovine heart mitochondria. Biochim. Biophys. Acta, 2003;1604:135–150.
7. Kmita K, Zickermann, V. Accessory subunit of mitochondrial complex I. Biochem. Soc. Trans. 2013; 41:1272-1279.
8. Stroud DA, Surgenor EE, Formosa LE, et al. Accessory subunits are integral for assembly and function of human mitochondrial complex I. Nature. 2016;538:123-126.
9. Pryde, KR, Hirst J. Superoxide is produced by the reduced flavin in mitochondrial complex I: A single, unified mechanism that applies during both forward and reverse electron transfer. *J. Biol. Chem.* 2011;286:18056-18065.
10. Treberg, JR, Quinlan CL, Brand MD. Evidence for two sites of superoxide production by mitochondrial NADH-ubiquinone oxidoreductase (complex I). *J. Biol. Chem*. 2011;286: 27103-27110.
11. Robb EL, Hall AR, Prime TA, et al. Control of mitochondrial superoxide production by reverse electron transport at complex I. *J. Biol. Chem*. 2018;293:9896-9879.

12. Shapira AH. Human complex I defects in neurodegenerative diseases. Biochim. Biophys. Acta. 1998;1364:261–270.

13. Dawson TM, Dawson VL. Molecular pathways of neurodegeneration in Parkinson's disease. Science. 2003;302;819–822.

14. Langston JW, Ballard P, Tetrud JW, et al. Chronic Parkinsonism in humans due to a product of meperidine-analog synthesis. *Science* 1983;219:979-980.

15. Betarbet R, Sherer TB, MacKenzie G, et al. Chronic systemic pesticide exposure reproduces features of Parkinson's disease. *Nat. Neurosci*. 2000;3:1301-1306.

16. Chouchani ET, Methner C, Nadtochiy SM, et al. Cardioprotection by S-nitrosation of cysteine switch on mitochondrial complex I. Nat. Med. 2013;19:753-759.

17. Chouchani ET, Pell VR, Gaude E, et al. Ischemic accumulation of succinate controls reperfusion injury through mitochondrial ROS. Nature. 2014;515:431-435.

18. Miyoshi H. Structure-activity relationship of some complex I inhibitors. Biochim. Biophys. Acta. 1998;1364:236-244.

19. Murai M, Miyoshi H. Current topics on inhibitors of respiratory complex I. Biochim. Biophys. Acta. 2016;1857:884-891.

20. Clark JM, Yamaguchi I. Scope and Status of Pesticide Resistance. In: J.M. Clark, I. Yamaguchi Editors. Agrochemical Resistance: Extent, Mechanism, and Detection. Washington DC: American Chemical Society; 2002. p. 1–22.

21. Ōmura S, Miyadera H, Ui H, et al. Anthelmintic compound, nafuredin, shows selective inhibition of complex I in helminth mitochondria, Proc. Natl. Acad. Sci. U. S. A. 2001:98;60–62.

22. Owen MR, Doran E, Halestrap AP. Evidence thatmetformin exerts its anti-diabetic effects through inhibition of complex 1 of the mitochondrial respiratory chain, Biochem. J. 2000:348;607–614.

23. El-Mir MY, Nogueira V, Fontaine E, et al. Dimethylbiguanide inhibits cell respiration

via an indirect effect targeted on the respiratory chain complex I, J. Biol. Chem. 2000:275;223–228.

24. Kelly B, Tannahill GM, Murphy MP et al. Metformin inhibits the production of reactive oxygen species from NADH:ubiquinone oxidoreductase to limit induction of IL-1β, and boosts IL-10 in LPS-activated macrophages. J. Biol. Chem. 2015;290:20455–20465.
25. Molina JR, Sun, Y, Protopopova M, et al. An inhibitor of oxidative phosphorylation exploits cancer vulnerability. Nat. Med. 2018:24;1036-1046.
26. Hatanaka Y, Sadakane Y. Photoaffinity labeling in drug discovery and developments: chemical gateway for entering proteomic frontier. Curr Top Med Chem. 2002:2; 271-288.
27. Weber T, Brunner J. 2-(Tributylstannyl)-4-[3-(trifluoromethyl)-3H-diazirin-3-yl] benzyl alcohol: a building block for photolabeling and crosslinking reagents of very high specific radioactivity. *J. Am. Chem. Soc.* 1995:*117*;3084-3095.
28. Murai M, Ishihara A, Nishioka T, et al. The ND1 subunit constructs the inhibitor binding domain in bovine heart mitochondrial complex I. Biochemistry. 2007:46;6409-6416.
29. Murai M, Sekiguchi K, Nishioka T, et al. Characterization of the inhibitor binding site in mitochondrial NADH-ubiquinone oxidoreductase using a quinazoline-type inhibitor, Biochemistry. 2009:48;688-698.
30. Sekiguchi K, Murai M, Miyoshi H. Exploring the binding site of acetogenin in the ND1 subunit of bovine mitochondrial complex I, Biochim. Biophys. Acta (Bioenergetics). 2009:1787;1106-1111.
31. Yamamoto S, Abe M, Nakanishi S, et al. Synthesis and characterization of photoaffinity probe of acetogenin, a strong inhibitor of mitochondrial complex I, Tetrahedron Lett. 2011:52;3090-3093.

32. Nakanishi S, Abe M, Yamamoto S, et al. Bis-THF motif of acetogenin binds to the third matrix-side loop of ND1 subunit in mitochondrial NADH-ubiquinone oxidoreductase, Biochim. Biophys. Acta (Bioenergetics). 2011:1807;1170-1176.

33. Murai M, Mashimo Y, Hirst J. Exploring interactions between the 49 kDa and ND1 subunits in mitochondrial NADH-ubiquinone oxidoreductase (complex I) by photoaffinity labeling, Biochemistry. 2011:50;6901-6908.

34. Shiraishi Y, Murai M, Sakiyama N, Fenpyroximate binds to the interface between PSST and 49 kDa subunit in mitochondrial NADH-ubiquinone oxidoreductase, Biochemistry. 2011:51;1953-1963.

35. Okun JG, Lümmen P, Brandt U. Three classes of inhibitor share a common binding domain in mitochondrial complex I (NADH-ubiquinone oxidoreductase). J. Biol. Chem. 1999:274:2625-2630.

36. Ino T, Nishioka T, Miyoshi H. Characterization of inhibitor binding sites of mitochondrial complex I using fluorescent inhibitor. Biochim. Biophys. Acta. 2003:1605;15-20.

37. Yamashita T, Ino T, Miyoshi H. et al. Rhodoquinone reaction site of mitochondrial complex I in parasitic helminth *Ascaris suum.*Biochim. Biophys. Acta 2004:1608;97–103.

38. Baradaran R, Berrisford JM, Minhas GS et al. Crystal structure of the entire respiratory complex I. Nature 2013:494;443-448.

39. Kleyman TR, Cragoe EJ. Amiloride and its analogs as tools in the study of ion transport. J. Membr. Biol. 1988:105;1-21.

40. Putney LK, Denker SP, Barber DL. The changing face of the Na+/H+ exchanger, NHE: structure, regulation, and cellular actions. Annu. Rev. Pharmacol. Toxicol. 2002:42;527-552.

41. Nakamaru-Ogiso E, Seo BB, Yagi T, et al. Amiloride inhibition of the proton-

translocating NADH-quinone oxidoreductase of mammals and bacteria, FEBS Lett. 2003:549;43-46.

42. Stolpe S, Friedrich T. The Escherichia coli NADH-ubiquinone oxidoreductase (complex I) is a primary proton pump but may be capable of secondary sodium antiport, J. Biol. Chem. 2004:279;18377-18383.

43. Mathiesen C, Hägerhäll C. Transmembrane topology of the NuoL, M, and N subunits of NADH:quinone oxidoreductase and their homologues among membrane-bound hydrogenases and *bona fide* antiporters, *Biochim. Biophys. Acta* 2002:1556;121-132.

44. Morino M, Natsui S, Ono T, et al. Single site mutations in the hetero-oligomeric Mrp antiporter from alkaliphilic *Bacillus pseudofirmus* OF4 that affect Na^+/H^+ antiport activity, sodium exclusion, individual Mrp protein levels, or Mrp complex formation. J. Biol. Chem. 2010:285;30942－30950.

45. Murai M, Habu S, Murakami S, et al. Production of new amilorides as potent inhibitors of mitochondrial respiratory complex I, Biosci. Biotechnol. Biochem. 2015:79;1061-1066.

46. Uno S, Kimura, H, Murai M, et al. Exploring the quinone/inhibitor-binding pocket in mitochondrial respiratory complex I by chemical biology approaches, J. Biol. Chem. 2019:294;679-696.

47. Ito T, Murai M, Morisaka H, et al. Identification of the binding position of amilorides in the quinone binding pocket of mitochondrial complex I, Biochemistry 2015:54;3677-3686.

48. Zickermann V, Wirth C, Nasiri H, et al. Mechanistic insight from the crystal structure of mitochondrial complex I. Science 2015:347;44-49.

49. Vinothkumar KR, Zhu J, Hirst J. Architecture of mammalian respiratory complex I. Nature 2014:515;80-84.

50. Zhu J, Vinothkumar KR, Hirst J. Structure of mammalian respiratory complex I.

Nature 536:2016;354-358.

51. Blaza JN, Vinothkumar KR, Hirst J. Structure of the deactive state of mammalian respiratory complex I. Structure 2018:26;312-319.

52. Fiedorczuk K, Letts JA, Degliesposti G, et al. Atomic structure of the entire mammalian mitochondrial complex I. Nature 2016:538;406-410.

53. Wu M, Gu J, Guo R, et al. Structure of mammalian respiratory supercomplex $I_1III_2IV_1$. Cell 2016:167;1598-1609.

54. Agip A-N A, Blaza JN, Bridges HR, et al. Cryo-EM structures of complex I from mouse heart mitochondria in two biochemically defined states. Nat. Struc. Mol. Biol. 2018:25;548-556.

55. Guo R, Zong S, Wu M, et al. Architecture of human mitochondrial respiratory megacomplex $I_2III_2IV_2$. Cell 2017:170;1247-1257.

56. Sharma V, Belevich G, Gamiz-Hernandez A P, et al. Redox-induced activation of the proton pump in the respiratory complex I. Proc. Natl. Acad. Sci. USA. 2015:122; 11571-11576.

57. Luca AD, Gamiz-Hernandez AP, Kaila VRI. Symmetry-related proton transfer pathways in respiratory complex I. Proc. Natl. Acad. Sci. USA. 2017:114;6314-6321.

58. Gamiz-Hernandez AP, Jussupow A, Johansson MP, et al. Terminal electron-proton transfer dynamics in the quinone reduction of respiratory complex I. J. Am. Chem. Soc. 2017:139;16282-16288.

59. Tsukiji S, Miyagawa M, Takaoka Y, et al. Ligand-directed tosyl chemistry for protein labeling in vivo. Nat. Chem. Biol. 2009:5;341−343.

60. Masuya T, Murai M, Morisaka H, et al. Pinpoint chemical modification of Asp160 in the 49 kDa subunit of bovine mitochondrial complex I via a combination of ligand-directed tosyl chemistry and click chemistry, Biochemistry 2014:53;7816-7823.

61. Wang Q, Chan TR, Hilgraf R, et al. Bioconjugation by copper(I)-catalyzed

azidealkyne [3+2] cycloaddition. J. Am. Chem. Soc. 2003:125;3192−3193.

62. Chang PV, Prescher JV, Sletten EM, et al. Copper-free click chemistry in living animals. Proc. Nat. Acad. Sci. U S A. 2010:107;1821-1826.

63. Jewett JC, Bertozzi CR. Cu-free click cycloaddition reactions in chemical biology. Chem. Soc. Rev. 2010:39;1272−1279.

64. Blackman ML, Royzen M, Fox JM. Tetrazine ligation: Fast bioconjugation based on inverse-electron-demand Diels-Alder reactivity. J. Am. Chem. Soc. 2008:130; 13518−13519.

65. Patterson DM, Nazarova LA, Xie B, et al. Functionalized cyclopropenes as biorthogonal chemical reporters. J. Am. Chem. Soc. 2012:134;18638−18643.

66. Masuya T, Murai M, Ito T, et al. Pinpoint chemical modification of the quinone-access channel of mitochondrial complex I via a two-step conjugation reaction, Biochemistry 2017:56;4279-4287.

67. Pravda L, Sehnal D, Toušek D, et al. MOLE online: a web-based tool for analyzing channels, tunnels and pores (2018 update). Nucleic Acids Res. 2018:46;W368-W373.

Figure legends

Figure 1. The entire structure of respiratory complex I. (a) The X-ray crystallographic structure of complex I from *T. thermophilus* (PDB entry 4HE8, ref. *38*). The subunits are named according to the nomenclature of bovine complex I. The binding pocket of quinone/inhibitor in complex I is located at the interfacial region between the hydrophilic and membrane domains, which is composed of the 49-kDa, PSST, and ND1 subunits (colored in *pink, blue,* and *orange,* respectively). In the magnified view, the proposed quinone-access channel and entrance of quinone (Q) are denoted by a dark column and red arrow, respectively. The terminal Fe-S cluster N2, which donate electrons to quinone, is also approximately 30 Å away from the entrance. The position of 49-kDa Asp160, which is specifically modified by acetogenin ligands (AL2 and AL6, see in Figure 4), are marked by a *dotted red circle*. (b) The cryo-EM structure of ovine complex I (PDB entry 5LNK, ref. *52*). The accessory subunits are colored in gray. The quinone-access channel proposed in ovine complex I was generated using MOLE (*67*) and is shown in black. The nomenclatures for the core subunits of complex I from various species are presented in Table S1.

Figure 2. Structures of complex I inhibitors and their photoreactive analogues. (a) Structures of bullatacin (a member of natural acetogenins) and photoreactive acetogenins ([^{125}I]TDA and [^{125}I]DANA), possessing a photolabile phenyl diazirine in place of the toxophoric γ-lactone ring and a small diazirine in the vicinity of the toxopholic bis-THF ring moiety, respectively. (b) Structures of aminoquinazoline (AQ) and photoreactive quinazoline ([^{125}I]AzQ), possessing a photolabile azido group on the toxophoric quinazoline ring. (c) Structures of fenpyroximate and photoreactive fenpyroximates ([^{125}I]APF and [^{125}I]AIF), possessing a photoreactive azido group at and far from the toxophoric pyrazole ring moiety, respectively. (d) Structures of photoreactive amilorides, possessing a photolabile azido group in the toxophoric pyrazinoyl ring ([^{125}I]PRA4 and [^{125}I]PRA6) or in the side chain moiety ([^{125}I]PRA3 and [^{125}I]PRA5), respectively. [^{125}I]PRA3 and [^{125}I]PRA4 are prototypical guanidine-type amilorides such as commercially available EIPA, MIA, and benzamil, while [^{125}I]PRA5 and [^{125}I]PRA6 are amide-type amilorides that elicit more potent inhibitory activities with bovine complex I.

Figure 3. An overview of the binding site of various quinone-site inhibitors in mitochondrial complex I. The 49-kDa, PSST, ND1, and 39-kDa subunits in ovine complex I (PDB entry 5LNK, ref. *52*) are colored in *pink*, *blue*, *orange*, and *green*, respectively. The quinone/inhibitor-access channel predicted in the current models is shown in black. (a) The regions labeled by photoreactive acetogenins, quinazoline, and fenpyroximates. The labeled regions are shown in *spheres*: The region spanning TMH4-5 (Val144-Glu192) and the loop connecting TMH5-6 (Thr201-Ala217) of the ND1 subunit (labeled by [^{125}I]TDA and [^{125}I]DANA, presented in yellow and orange, respectively); The N-terminal region (Val44-Arg63) of the 49-kDa subunit and the loop connecting TMH5-6 of the ND1 subunit (labeled by [^{125}I]AzQ presented in light pink and orange, respectively); Ser43−Arg66 of the PSST subunit (labeled by [^{125}I]APF, presented in blue) and Asp160−Arg174 of the 49-kDa subunit (labeled by [^{125}I]AIF, presented in deep pink). The regions labeled by each inhibitors are also shown in Figure S1. (b) The regions labeled by photoreactive amilorides. The labeled regions are shown in *spheres*: The N-terminal region (Val-44–Glu-67) of the 49-kDa subunit (labeled by [^{125}I]PRA4, [^{125}I]PRA5, and [^{125}I]PRA6, presented in *pink*); Leu33–Tyr67 of the PSST subunit (labeled by [^{125}I]PRA5, presented in *blue*); the loop connecting TMH5-6 (Thr201–Ala217) of the ND1 subunit (labeled by[^{125}I]PRA6, presented in *orange*); and Thr227–Pro252 and Pro277–Lys283 of the 39-kDa subunit (labeled by [^{125}I]PRA3, presented in *green*). The yellow circle marks the putative entry area to the open binding pocket for the quinone/inhibitor. In ovine complex I (ref. *52*), Asp41–Leu43 and Phe253–Glu276 in the 49- and 39-kDa subunits, respectively, were not modeled.

Figure 4. Schematic diagram of the pinpoint modification of the 49-kDa Asp160 located inside the quinone-access channel of bovine mitochondrial complex I.

(a) The position of 49-kDa Asp160 (marked by a *dotted red circle*) in the proposed quinone-access channel in ovine complex I (PDB entry 5LNK). The 49-kDa subunit is colored in *pink*. (b) The 49-kDa Asp160 can be modified by externally added bulky tags such as TAMRA-DIBO and BODIPY-tetrazine through the two-step conjugation procedures (refs. *60* and *66*).

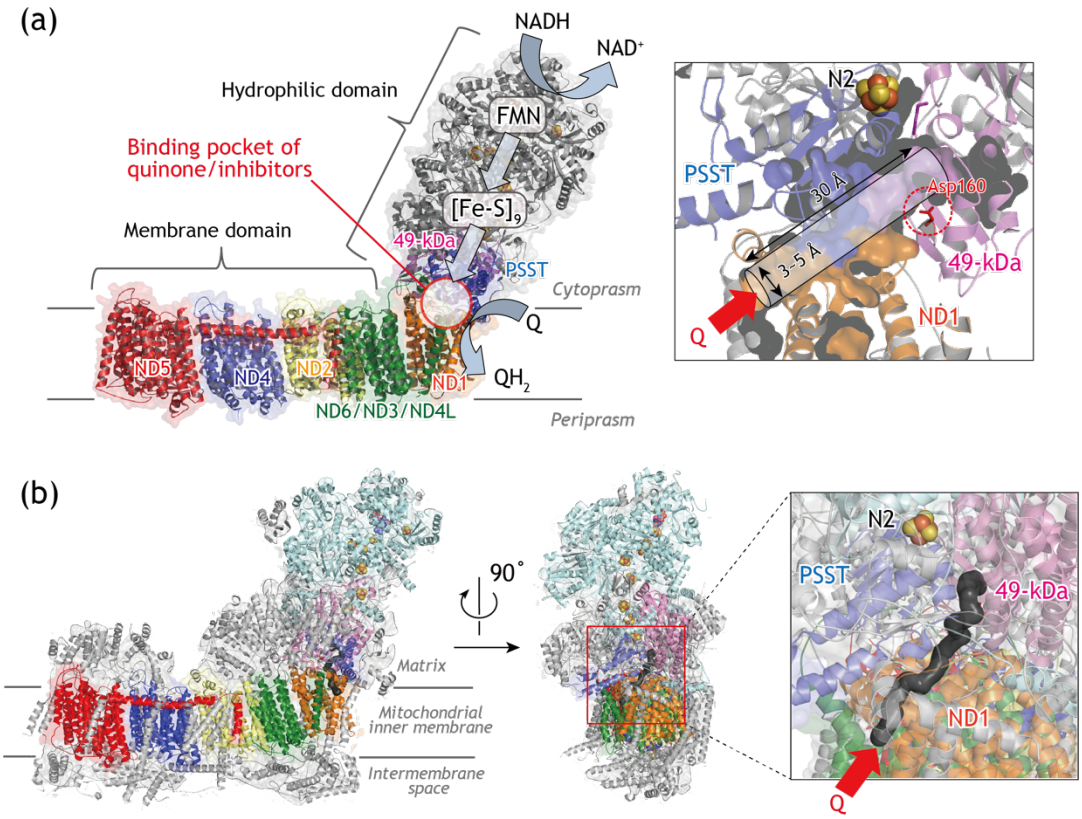
(a)
NADH
NAD+
Hydrophilic domain
FMN
Binding pocket of
quinone/inhibitors
[Fe-S]9
Membrane domain
49-kDa
PSST
Cytoprasm
Q
QH2
ND5
ND4
ND2
ND1
ND6/ND3/ND4L
Periprasm
N2
PSST
30 Å
Asp160
3-5 Å
49-kDa
ND1
Q
(b)
90°
Matrix
Mitochondrial
inner membrane
Intermembrane
space
N2
PSST
49-kDa
ND1
Q

Figure 1

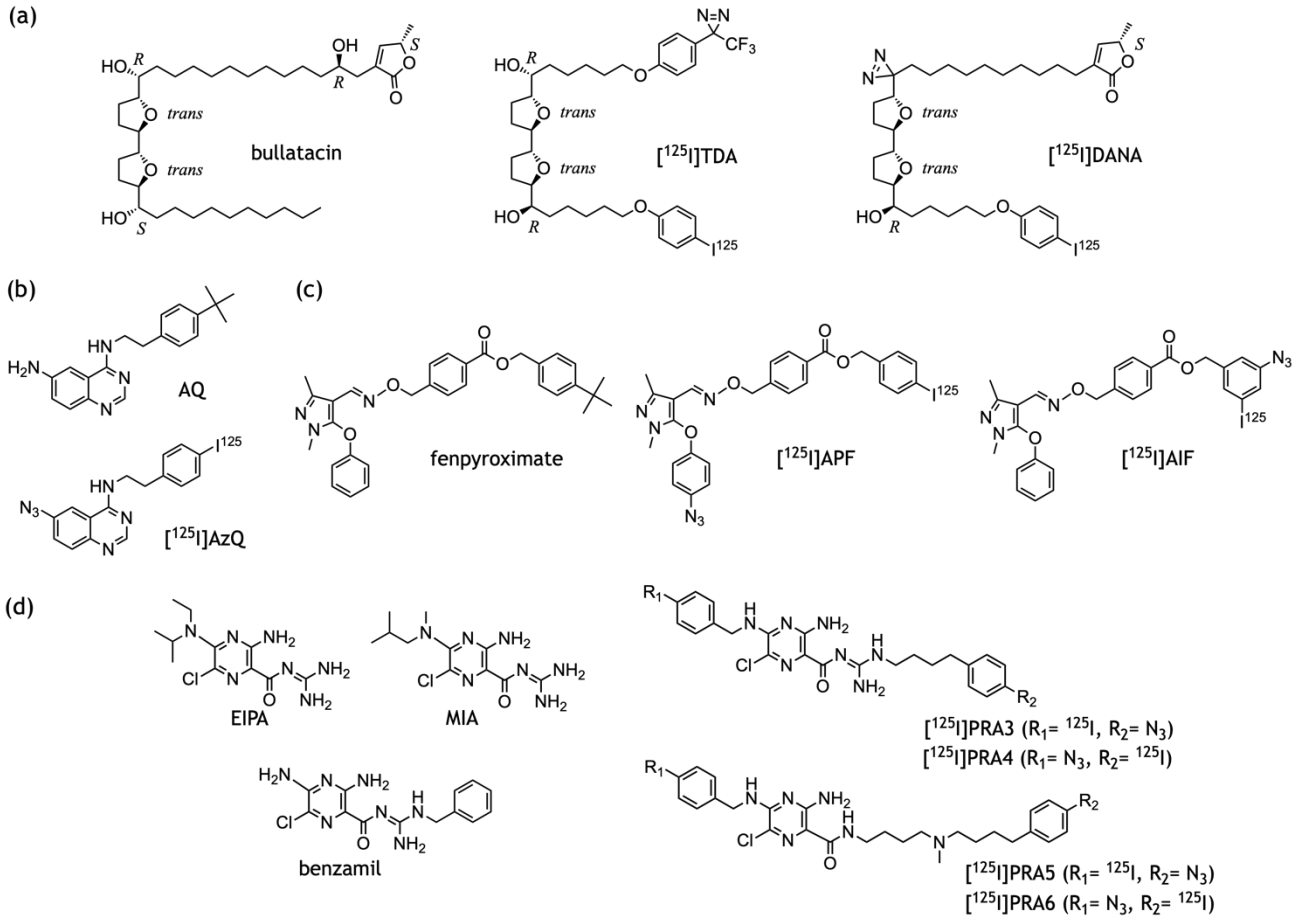
(a)
bullatacin
[125I]TDA
[125I]DANA
(b)
AQ
[125I]AzQ
(c)
fenpyroximate
[125I]APF
[125I]AIF
(d)
EIPA
MIA
benzamil
[125I]PRA3 (R1= 125I, R2= N3)
[125I]PRA4 (R1= N3, R2= 125I)
[125I]PRA5 (R1= 125I, R2= N3)
[125I]PRA6 (R1= N3, R2= 125I)

Figure 2

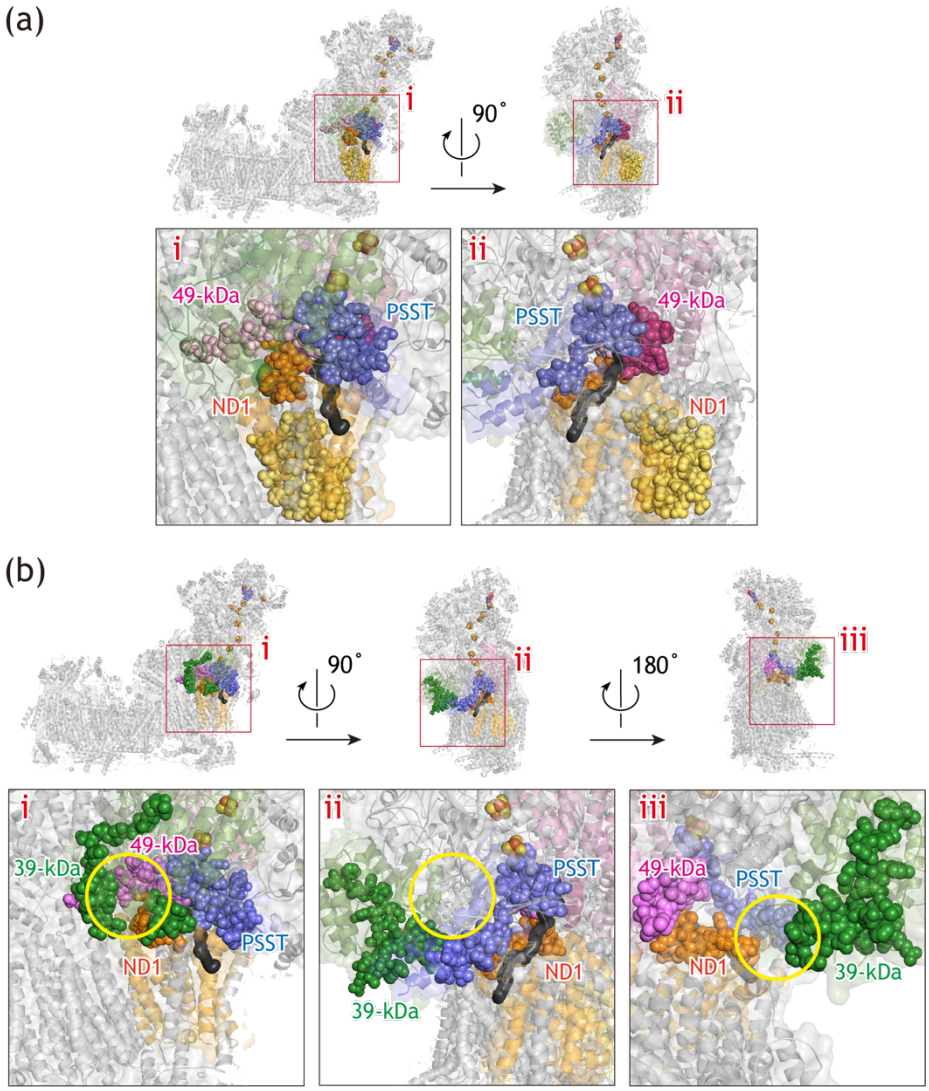
(a)
i
ii
90˚
i
49-kDa
PSST
ND1
ii
PSST
49-kDa
ND1
(b)
i
90˚
ii
180˚
iii
i
49-kDa
39-kDa
PSST
ND1
ii
PSST
ND1
39-kDa
iii
49-kDa
PSST
ND1
39-kDa

Figure 3

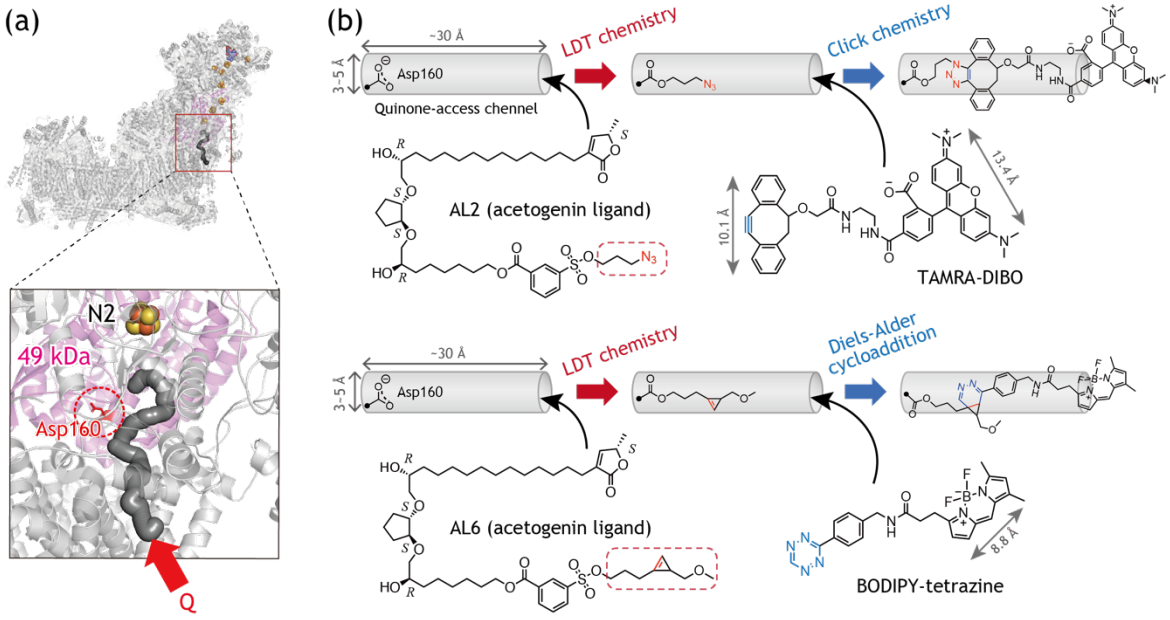
(a)
N2
49 kDa
Asp160
Q
(b)
~30 Å
3–5 Å
Asp160
Quinone-access chennel
LDT chemistry
Click chemistry
AL2 (acetogenin ligand)
10.1 Å
13.4 Å
TAMRA-DIBO
LDT chemistry
Diels-Alder cycloaddition
AL6 (acetogenin ligand)
8.6 Å
BODIPY-tetrazine

Figure 4